Size-Dependent Changes in Sea Spray Aerosol Composition and Properties with Different Seawater Conditions

ARTICLE *in* ENVIRONMENTAL SCIENCE & TECHNOLOGY · MAY 2013

Impact Factor: 5.33 · DOI: 10.1021/es400416g · Source: PubMed

13 AUTHORS, INCLUDING:

Douglas B Collins
University of California, San Diego
17 PUBLICATIONS **157** CITATIONS
SEE PROFILE

Defeng Zhao
Forschungszentrum Jülich
22 PUBLICATIONS **267** CITATIONS
SEE PROFILE

Kim Prather
University of California, San Diego
296 PUBLICATIONS **9,844** CITATIONS
SEE PROFILE

Environmental Science & Technology

Article

pubs.acs.org/est

Size-Dependent Changes in Sea Spray Aerosol Composition and Properties with Different Seawater Conditions

Andrew P. Ault,[†] Ryan C. Moffet,[‡] Jonas Baltrusaitis,[†] Douglas B. Collins,[§] Matthew J. Ruppel,[§] Luis A. Cuadra-Rodriguez,[§] Defeng Zhao,[§] Timothy L. Guasco,[§] Carlena J. Ebben,[∥] Franz M. Geiger,[∥] Timothy H. Bertram,[§] Kimberly A. Prather,[§,⊥,*] and Vicki H. Grassian[†,*]

[†]Department of Chemistry, University of Iowa, Iowa City, Iowa, 52242, United States

[‡]Department of Chemistry, University of the Pacific, Stockton, California, 95211, United States

[§]Department of Chemistry and Biochemistry, University of California, San Diego, La Jolla, California, 92037, United States

[∥]Department of Chemistry, Northwestern University, Evanston, Illinois, 60208, United States

[⊥]Scripps Institution of Oceanography, University of California—San Diego, La Jolla, California, 92093, United States

Supporting Information

ABSTRACT: A great deal of uncertainty exists regarding the chemical diversity of particles in sea spray aerosol (SSA), as well as the degree of mixing between inorganic and organic species in individual SSA particles. Therefore, in this study, single particle analysis was performed on SSA particles, integrating transmission electron microscopy with energy dispersive X-ray analysis and scanning transmission X-ray microscopy with near edge X-ray absorption fine structure spectroscopy, with a focus on quantifying the relative fractions of different particle types from 30 nm to 1 μm. SSA particles were produced from seawater in a unique ocean-atmosphere facility equipped with breaking waves. Changes to the SSA composition and properties after the addition of biological (bacteria and phytoplankton) and organic material (ZoBell growth media) were probed. Submicrometer SSA particles could be separated into two distinct populations: one with a characteristic sea salt core composed primarily of NaCl and an organic carbon and Mg^{2+} coating (SS-OC), and a second type consisting of organic carbon (OC) species which are more homogeneously mixed with cations and anions, but not chloride. SS-OC particles exhibit a wide range of sizes, compositions, morphologies, and distributions of elements within each particle. After addition of biological and organic material to the seawater, a change occurs in particle morphology and crystallization behavior associated with increasing organic content for SS-OC particles. The fraction of OC-type particles, which are mainly present below 180 nm, becomes dramatically enhanced with increased biological activity. These changes with size and seawater composition have important implications for atmospheric processes such as cloud droplet activation and heterogeneous reactivity.

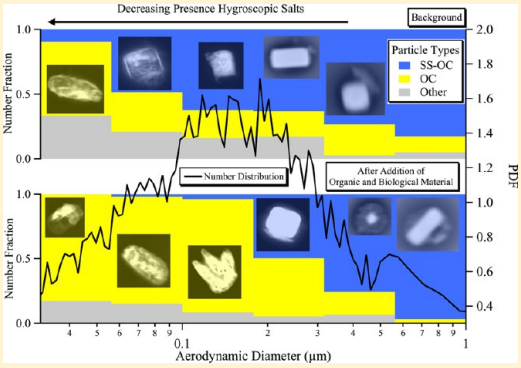

INTRODUCTION

Breaking waves, formed through wind-driven mechanisms, that generate sea spray aerosol (SSA) in marine environments via bubble bursting represent one of the largest fluxes of aerosol particles into the atmosphere.[1] As such, SSA has a significant impact on the earth's radiative balance by scattering light and acting as the nuclei of cloud droplets and ice crystals, thus influencing the properties of clouds.[2] Understanding the factors which control SSA hygroscopicity, cloud condensation nuclei (CCN) activity, and heterogeneous reactivity is critical to predicting their radiative effects on a global scale through climate modeling.[3−6] A key determinant of these climate properties is the chemical composition of single particles, and considerable effort in recent years has focused on describing SSA chemical composition from a single particle perspective.[3,7] In addition to inorganic salts, studies have pointed to organic carbon species in the ocean as an important contributor to the ejected aerosol.[4,8−12] A great deal of uncertainty remains regarding the degree of mixing between inorganic and organic species within individual SSA particles.[3,7]

Although great strides have been made in understanding organic matter in seawater and its transfer to the atmosphere in aerosols over the past few decades,[3,4,9,13] many of the different organic compounds dissolved in seawater remain uncharacterized.[14] Studies on seawater have identified colloids, marine aggregates, or gels as significant contributors to particulate organic matter (POM).[13,15−20] Chemical characteristics of POM include aliphatic and carbohydrate components, along with cations and inorganic components.[14,16,18] When waves

Received: January 27, 2013
Revised: April 26, 2013
Accepted: May 2, 2013
Published: May 2, 2013

break in regions which contain organic species, including both POM and dissolved organic matter (DOM), water insoluble organic carbon is a significant fraction of SSA particle mass, particularly with decreasing particle size.[9,10,12,21] This ejected organic-enriched SSA has received attention due to its low water uptake compared with inorganic salts and its potential to alter CCN activity or heterogeneous reactivity of the SSA population.[22,23] In the key size range for particles involved in cloud formation, from ca. 50 to 150 nm, many studies show organic compounds contributing to greater than 75% of the total mass of SSA particulate matter,[9,10,12] however little is known as to how this mass is distributed among individual particles.

An important finding has been that many of the smaller particles in the CCN size range do not contain hygroscopic salts.[24] This has led to the hypothesis that salts do not exist below 200 nm,[24] though other studies support their existence.[25,26] As these different studies have shown, organic matter can exist both as an internal mixture with hygroscopic salts (both species in a single particle)[27] or as a separate, externally mixed population with no hygroscopic material in the particles.[24] As many of these studies merely describe different types qualitatively,[24] a critical step toward understanding the properties of SSA particles across the full size range (down to 30 nm) involves additional quantitative analysis of the relative contributions of the different mixing states of SSA particles, as shown below.

Another potentially critical factor that determines the mixing state of SSA is the composition of the seawater.[28,29] For example, SSA generated using seawater with low concentrations of total organic carbon or biological species have very different properties than aerosol generated from seawater with higher concentrations of total organic carbon and biological material, which leads to changes in the overall climate impacts of these particles that need to be better understood.[9,29,30]

To systematically study the composition and structure of SSA in an isolated system, a focus of the Center for Aerosol Impacts on Climate and the Environment (CAICE), a series of experiments were conducted at a unique ocean-atmosphere wave flume facility, which uses breaking waves to generate SSA with bubble-size distributions representative of the open ocean.[28,31] Prather et al. provides an overview and overarching link between seawater composition, SSA generated, and SSA climate-relevant properties.[28] Here, a detailed analysis of SSA particles using off-line methods is presented. In particular, we use multiple microscopy and spectroscopy techniques to probe the variation in chemical composition, mixing state, and internal structure of SSA particles under a range of seawater conditions from 30 nm to 10 μm, with a focus on quantifying relative fractions of different particle types from 30 nm to 1 μm. The 30 nm to 10 μm size range includes the critical size ranges important for both cloud droplet activation and heterogeneous reactions. It is shown that systematically modified seawater conditions lead to changes in the contributions of different subpopulations of SSA particles as a function of size. In addition, it is shown that within each distinct particle population, variability exists in chemical composition, particle morphology, and phase state. These findings represent an important step forward in determining how changes in the characteristics of seawater chemistry and biology including total organic carbon, bacteria concentrations, and phytoplankton concentrations, can be transferred to SSA particles produced through wave action.

EXPERIMENTAL SECTION

CAICE Intensive Measurements. Details of the wave flume apparatus have been previously provided.[28] Briefly, seawater filtered through filter beds of No. 12 crystal sand taken in from the ocean floor at the end of the Scripps Institution of Oceanography (SIO) pier in La Jolla, CA (200 m off the coast) was pumped into a sealed glass channel 33 m by 1 m by 0.5 m in the SIO Hydraulics Laboratory filling the channel to 0.5 m. Nascent SSA particles were generated through the use of a hydraulic paddle forming waves at 0.6 Hz with an amplitude of 0.3 m that crested on a 2 m long "beach" extending from the base of the channel to the surface of the water at a 30° angle. During a mesocosm experiment, 4 additions of biological and organic material were made: (1) bacteria and ZoBell media (peptone, yeast extract, and glucose)[32] (0.6 days), (2) bacteria and ZoBell media (1.9 days), (3) ZoBell media (2.6 days), and finally, (4) bacteria, phytoplankton, and ZoBell media (2.8 days).[28] Seawater conditions in the wave flume were initially similar to typical ocean conditions, as discussed in Prather et al.,[28] from the beginning of the experiment until the last addition, at which point the indicators increased above mean ocean state (TOC = 60 to 70 μM, bacteria concentrations 5×10^5 to 3×10^6, and chlorophyll-*a* concentrations of 0.15 to 1.0 mg/m^3).[33−35] See the Supporting Information, SI, for additional details on the bacteria and ZoBell media used in this study.

Microscopy Sample Collection and Analysis. Samples analyzed in this study were collected using a multiple orifice uniform deposition impactor (MOUDI, MSP Corp. Model 100) sampling air at 30 lpm, with 50% size cuts at 5.6, 2.5, 1.0, 0.53, 0.30, 0.18, 0.09, and 0.05 μm. A variety of substrates were used, including: 400 mesh Carbon Type B/Formvar grids (Ted Pella Inc., part no. 01814-F) for transmission electron microscopy (TEM) and scanning transmission X-ray microscopy with near edge X-ray absorption fine structure (STXM-NEXAFS) spectroscopy and silicon wafers (Ted Pella Inc., part no. 16012) for scanning electron microscopy (SEM). TEM data were collected on a JEOL 2100f field emission TEM operating at 200 kV with a Gatan high angle annular dark field (HAADF) detector and a Thermo Noran Nano energy dispersive X-ray spectrometry (EDX) detector (Nanotrace, Thermo Inc.). SEM-EDX data were collected on a Hitachi S-3400N operating in variable pressure mode at 15 keV with a Thermo EDX detector. STXM/NEXAFS was conducted on beamlines 11.0.2 and 5.3.2.2 at the advanced light source at Lawrence Berkeley National Laboratory using previously described methodology.[36,37] Briefly, soft X-ray radiation was analyzed at the C (290 eV), Ca (352 eV), S (170 eV), and Cl (199 eV) absorption edges. X-ray energy was selected by a monochromator, and the transmitted energy (I) was measured as the sample was rastered using piezoelectric nanotranslators at different X-ray energies. The X-ray spectrum was converted to optical density using the Beer−Lambert Law, $OD = \ln(I_0/I) = \mu\rho t$, where μ is the mass absorption coefficient, ρ is the mass density, and t is the thickness.[36]

TEM Data Analysis. To quantify the size-resolved relative fractions of different subpopulations by merging different MOUDI stages, single particle size and chemical composition were determined for roughly 100 particles per stage for stages 4 through 8 (30−1000 nm). Particles were sized using ImageJ (http://imagej.nih.gov/im) by tracing the perimeter (P) manually, which also gave a 2-dimensional projection area

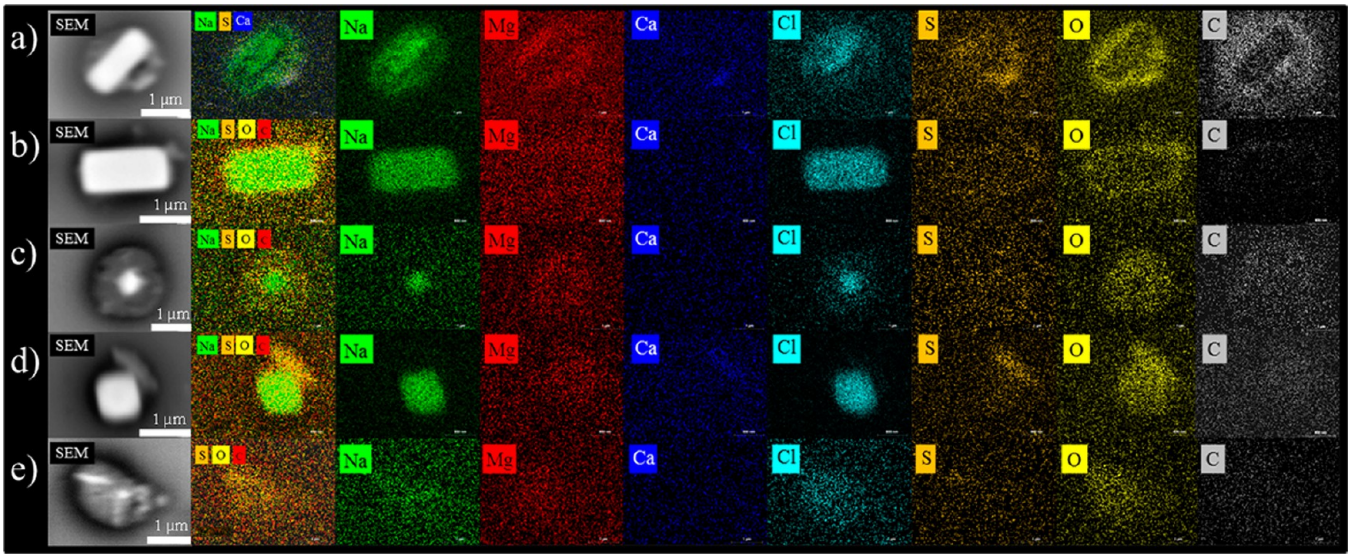

Figure 1. SEM-EDX images and elemental maps of representative particle types at or greater than 1 μm in diameter. These images and elemental maps show (a) a typical SS-OC particle with Mg, S, O, and C surrounding a NaCl core, (b) an SS-OC particle with a very thin Mg−C−O coating, (c) an SS-OC particle with a more extensive and thicker coating, (d) an SS-OC particle with a distinct rod containing Ca and S ($CaSO_4$), and (e) an SS-OC particle with all species internally mixed, lacking a defined NaCl core. See text for further discussion of the range of particles within this SS-OC type.

(A). For aqueous particles where an outer ring was present, indicating that an initially aqueous particle had subsequently effloresced, the outer perimeter was used to determine particle A. The projected area diameter (d_{pa}) of each particle (equivalent circle diameter using particle A)[38] was then converted to aerodynamic diameter (d_a) to allow for comparison with other methods,[28] through the equation:

$$d_a = \frac{d_{pa}}{S_V\sqrt{\frac{\rho_p}{S_D\rho_0}}} \quad (1)$$

where S_v is the volumetric shape factor, S_D is the aerodynamic shape factor (a value of 1 for aqueous/spherical particles), ρ_p is the particle density, and ρ_0 is unit density (1 g/cm^3).[39,40] Projected area diameter is related to the area a particle occupies on the substrate, while aerodynamic diameter is related to the particle settling velocity, which is important when considering atmospheric behavior. S_v is calculated from the following equation:

$$S_v = \frac{1}{C} = \frac{1}{4\pi\frac{A}{P^2}} \quad (2)$$

where C is the particle circularity ($C = 4\pi A/P^2$, where A and P are defined above). A ρ_p of 1.8 g/cm^3 was used for salt-containing particles and 1.2 g/cm^3 for organic particles without salts.[41,42] Size distributions for each stage were determined, and the relative contribution of each stage to a specific size bin, using 4 logarithmic bins per decade. The fractions of the different particle types were then weighted according to this contribution. As the samples are collected at ca. 60% relative humidity (RH) (above the efflorescence RH, the RH at which a particle dehydrates and recrystallizes), the diameter of the particle determined by the edge of the particle is considered the wet diameter, although due to spreading on impact, the diameter is an upper bound. TEM-EDX analysis is conducted under vacuum leading initially wet particles to effloresce and degas volatile components prior to analysis. Further information describing the number of particles analyzed by each technique, the sizing of particles, and merging of stages is given in the SI (Table S1 and Figure S1).

RESULTS AND DISCUSSION

Particles from 1 to 10 μm were investigated using SEM-EDX, whereas those below 1 μm were primarily analyzed with TEM-EDX and STXM-NEXAFS. Particles were classified into a variety of types; the fractional contribution and morphology of each type are presented as a function of size and seawater composition.

Analysis of Aerosol Particles At or Above 1 μm in Diameter. The vast majority of aerosols at or above 1 μm are internal mixtures of salts and organic material. Figure 1 shows SEM images and EDX elemental maps of representative particles within the 1 to 10 μm size range. Elemental mapping provides the ability to characterize the distribution of the elements within each particle and has become an important tool for off-line particle analysis in recent years.[43−45] Figure 1a shows a typical particle with an internal mixture containing an NaCl cubic core, a ring of organic carbon (OC), as seen in the C and O elemental maps, and a region with a localized distribution of Ca and S (discussed below). The partitioning that is observed here is typical of SSA particles analyzed previously that have undergone efflorescence.[46] This segregation is in part due to the fact that the insoluble components (OC species) precipitate as the particle dehydrates,[47] followed by crystallization of slightly soluble species ($CaSO_4$ and other sulfate species), and then crystallization of the most abundant species, NaCl. A ring with the most hygroscopic material, such as $MgCl_2$ and $KMgCl_3{\cdot}6H_2O$, effloresces last and forms an amorphous halo around the NaCl crystal under all observed conditions.[48,49] Particles in Figure 1 contain salts, organic matter, and sulfate, and are labeled as sea salt-organic carbon (SS−OC).

The amount of OC present and the thickness of the OC ring around the NaCl core vary substantially among SS-OC

dx.doi.org/10.1021/es400416g | Environ. Sci. Technol. 2013, 47, 5603−5612

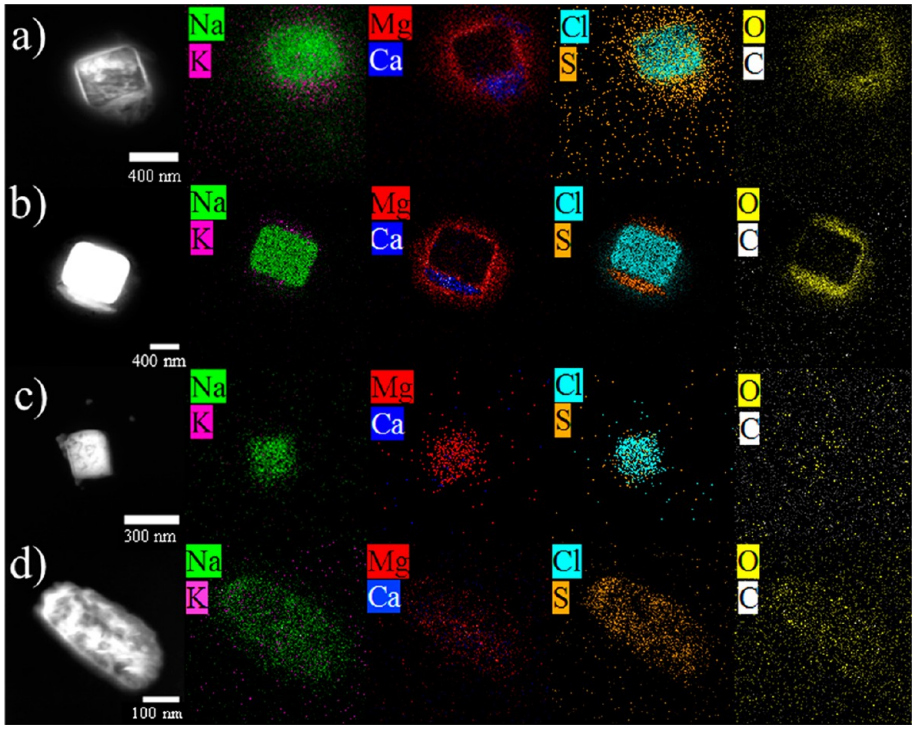

Figure 2. TEM images (dark field) and elemental maps of common particle types observed below 1 μm: (a) SS-OC with Ca and S not isolated to any specific region within the particle, (b) SS-OC with Ca−S rod structure ($CaSO_4$), (c) SS-OC with S and other cations distributed homogeneously throughout the particle, and (d) an OC particle which also contains inorganic elements including Na, Mg, Ca, and S but not Cl.

particles. While some particles have a very thin ring of C around the particle in the elemental maps (Figure 1b), others have a much thicker coating (Figure 1c). The amount of sulfur, as measured by the atomic percentage of the sulfur signal, also varies for different particles from less than 1% to 13%, with a median value of 2% (excluding carbon and oxygen signals due to substrate interference). For example, in Figure 1a, there is an isolated region where sulfur, most likely in the form of sulfate (vide infra), is seen, whereas for other particles there is a clearly crystalline Ca−S (also sulfate) rod (Figure 1d). For some particles, all of the elements present are distributed homogeneously throughout the particle (Figure 1e). The observed variation in the amount of OC present has important implications for how the particles will take up water and undergo heterogeneous reactions, such as those with N_2O_5.[50]

Analysis of Aerosol Particles Below 1 μm in Diameter. Particles below 1 μm in diameter can be classified into two main groups: internal mixtures containing NaCl, $MgCl_2$, sulfate species, and organic carbon species (SS-OC) and a separate group of organic carbon particles which contains cations and anions, but no chloride and, thus, no NaCl core. This is seen in the dark field transmission electron microscopy (TEM) images and elemental maps in Figure 2. Several examples of SS-OC particles smaller than one micrometer in diameter are shown in Figure 2a−c, demonstrating the variability observed within SS-OC particle types. The most common type observed within this class contained a distinct NaCl cubic core, a ring of Mg and O, and a distinct region adjacent to the particle showing Ca and S in the elemental map (Figure 2a), similar to Figure 1a. Different structures of the NaCl cores were observed; varying from cubic to more rounded, and are discussed in detail below. Figure 2b shows a NaCl core with an Mg ring around the edge and a well-defined rod containing Ca and S, presumably $CaSO_4$, a particle morphology more typical of larger-supermicrometer particles as shown in Figure 1d. Figure 2c shows a particle where several elements are present (Mg, Ca, S, and K) that are distributed evenly throughout the particle core that also contained NaCl, as seen for larger particles in Figure 1e. Further information on the SS-OC particles is given in Figure 3 for particles less than

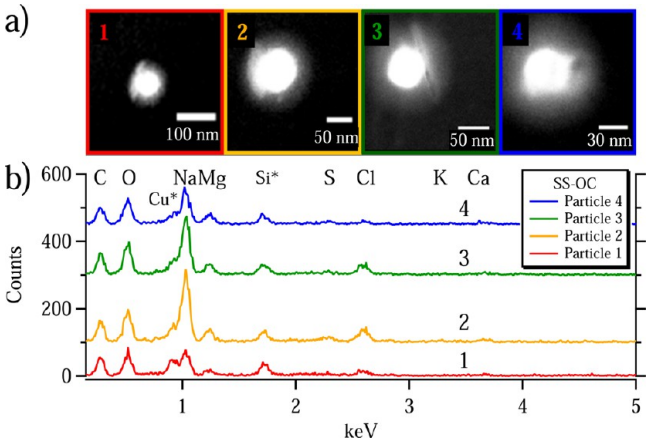

Figure 3. (a) Dark field TEM images of smaller SS-OC particles and (b) EDX spectra corresponding to the color box around each numbered particle. The * indicates substrate or artifact (Cu and Si), while C and O have contributions from both the substrate and the sample.

200 nm in diameter, with images for 4 particles and corresponding EDX spectra. The differences observed in the particles shown in Figure 2a−c, Figure 1a−e, and Figure 3 indicate that SS-OC particles across a broad size range (1 μm to 30 nm) have a significant amount of variability with respect to the concentrations and distribution of different species (e.g.,

dx.doi.org/10.1021/es400416g | Environ. Sci. Technol. 2013, 47, 5603−5612

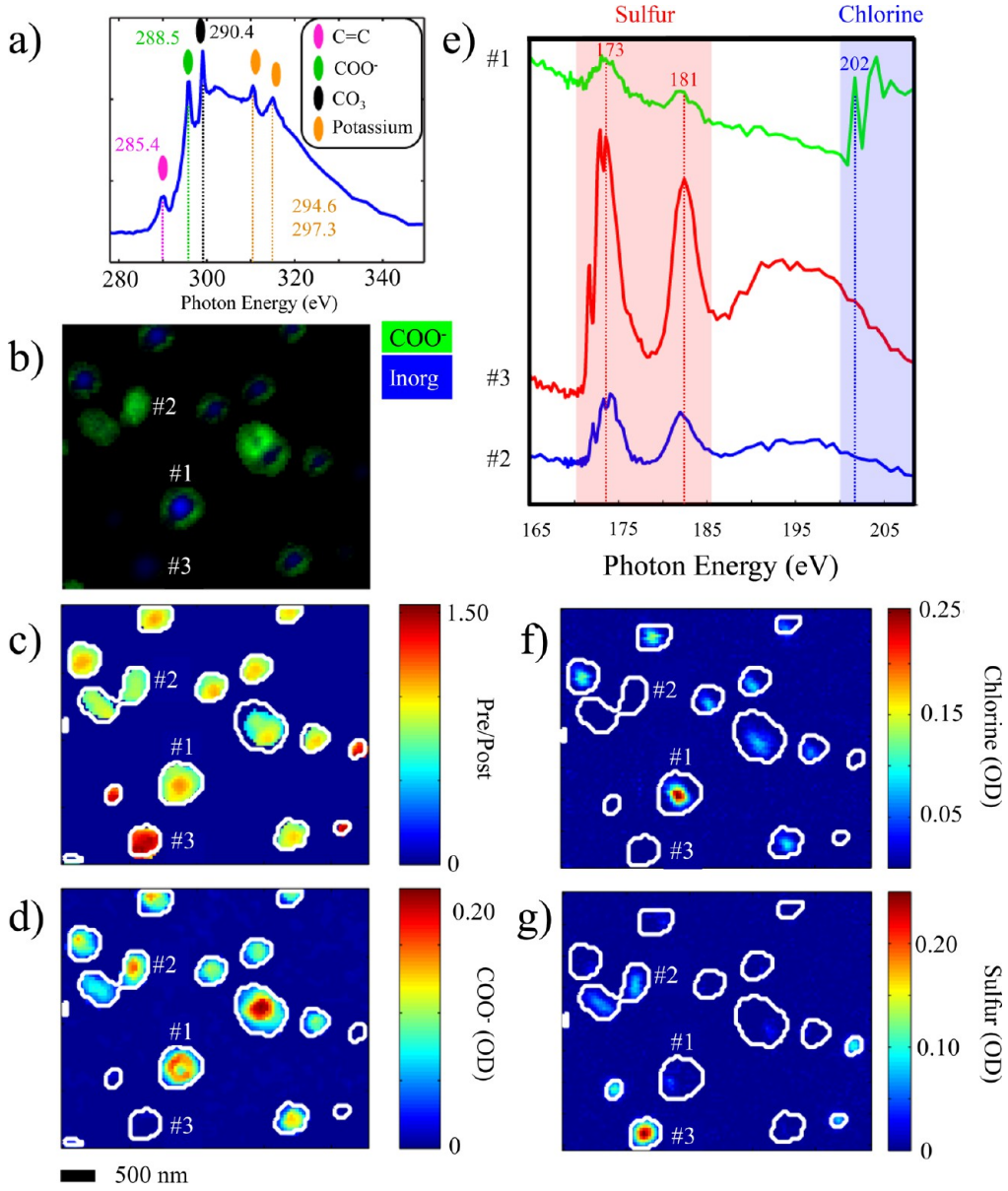

Figure 4. STXM-NEXAFS data for individual particle: (a) shows a typical NEXAFS spectrum at the carbon K-edge for a single particle observed below 500 nm in size, with peaks labeled for C═C at 285.4 eV, COO^- at 288.5 eV, and CO_3^{2-} at 290.4 eV, as well as nearby potassium L_3 at 294.6 and L_2 at 297.3 eV are seen; (b) Particle #1, "SS-OC" type, particle #2, "OC" type, and particle #3, a contamination type identified as ammonium sulfate – "AS" (particle 3 is discussed in more detail in the Supporting Information); more detailed analysis of the carbon K-edge with the colors representing a singular value decomposition (SVD) map combining COO^- concentration (green) and the inorganic-to-organic ratio (blue) for these three particles; (c) shows a map of the carbon K-edge pre-edge/postedge an indicator of inorganic intensity, (d) shows a map of COO^- optical density (OD), (e) NEXAFS spectra of the sulfur and chlorine L-edges (sulfur L_3 at 173 eV and L_2 at 181 eV and chlorine L_2 and 202 eV), (f) map of chlorine OD, and (g) map of sulfur OD.

different amounts of organic species, i.e., OC, as well as different amounts of sulfate). For these internal mixtures, it is seen that there is an increase in OC and a less cubic NaCl core with decreasing particle size.

As EDX is best-suited for analysis of the inorganic components in different particles, STXM-NEXAFS was used to provide more detail on the organic components present in SSA particles below 1 μm. Figure 4a shows a typical NEXAFS C spectrum with key components labeled. The most abundant peak observed throughout the different samples was COO^- or carboxylate groups (288.5 eV), along with minor peaks for C═C (285.4 eV) and CO_3^{2-} (290.4 eV), which appeared in a small fraction of SSA particles. The prominence of carboxylate groups agrees with previous analysis of particle phase organic matter in SSA particles by STXM.[51] In Figure 4b, particle 1 shows an SS-OC particle with an inorganic core and COO^- shell around it in a singular value decomposition map of COO^- and inorganic material.[36] The inorganic to organic ratio shown in Figure 4c supports an inorganic core, while the COO^- map in Figure 4d highlights the organic outer ring. Additionally, Figure 4e shows a NEXAFS spectrum of the S and Cl L-edge region with a clear peak for Cl above 200 eV and less intense peaks for S at 173 and 181 eV, corresponding to sulfate,[52,53] as also observed through Raman microspectroscopy.[54] Figure 4f shows the Cl as shown in Figure 4e concentrated in the core of the particle and Figure 4g shows a small amount of sulfur on the edge of the

dx.doi.org/10.1021/es400416g | Environ. Sci. Technol. 2013, 47, 5603–5612

particle, consistent with the presence of chloride and sulfate as discussed above. It should be noted that Cl-to-Na ratios have been shown to decrease as a function of decreasing size previously.[55]

As shown in Figure 2d, many particles observed below 1 μm in diameter did not contain a NaCl core; in this case the particle contains C and O throughout and is labeled OC. From EDX analysis, these particles also contain inorganic elements including S, Na, Mg, Ca, and K, but not Cl. Figure 5 shows

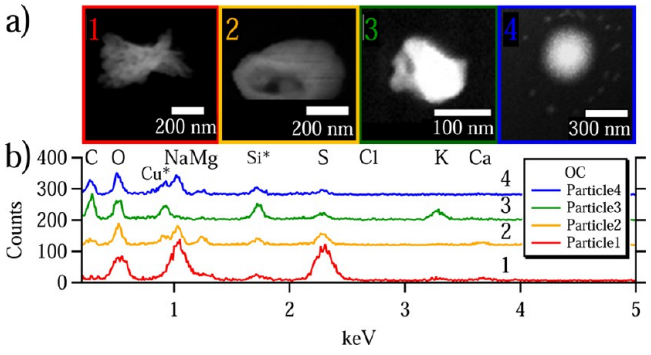

Figure 5. (a) Dark field TEM images of multiple OC particles and (b) EDX spectra corresponding to the color box around each numbered particle. The * indicates substrate or artifact (Cu and Si), while C and O have contributions from both the substrate and the sample.

TEM images and EDX spectra of four OC particles below 200 nm.[56] These particles have a wide range of morphologies suggesting they are not simply effloresced aqueous droplets. STXM identifies this particle type as having COO^- functionality comprising a large fraction of the organic content of the particle (Particle 2, Figure 4b), along with inorganic ions (Figure 4c). Additional spectra showing the variability of the C K-edge spectrum before and after addition of biological and organic material are given in the SI (Figure S2).

From Figure 4e, the particle S L-edge spectrum shows that S is primarily in the form of sulfate within OC particles at least in the size range of 200−500 nm.[52] This identifies the sulfur as mixed cation sulfate, as has been observed and identified for ambient samples.[57] This may come from sulfate in seawater, which is the second most abundant anion after chloride.[56] Additionally, a portion of the sulfate may initially be in the form of organic sulfur (such as in dimethylsulfoniopropionate, DMSP) and oxidized to sulfate on the substrate after collection. Furthermore, sulfate in these particle types is not on the edge of the particle (as for SS-OC), but rather in the center (Figure 4g).[58] Sulfur speciation for smaller sizes could be different as NEXAFS analysis was only done for particles >200 nm in diameter. NEXAFS data in this region also confirm that the OC type particles lack any detectable Cl as there is no peak present at ca. 200 eV (Figure 4e) in the spectrum, corroborating the absence of Cl in the EDX elemental map (Figure 4f).

Although Cl:Na ratios in NaCl have been shown to decrease as a function of decreasing particle size, this is not to the point

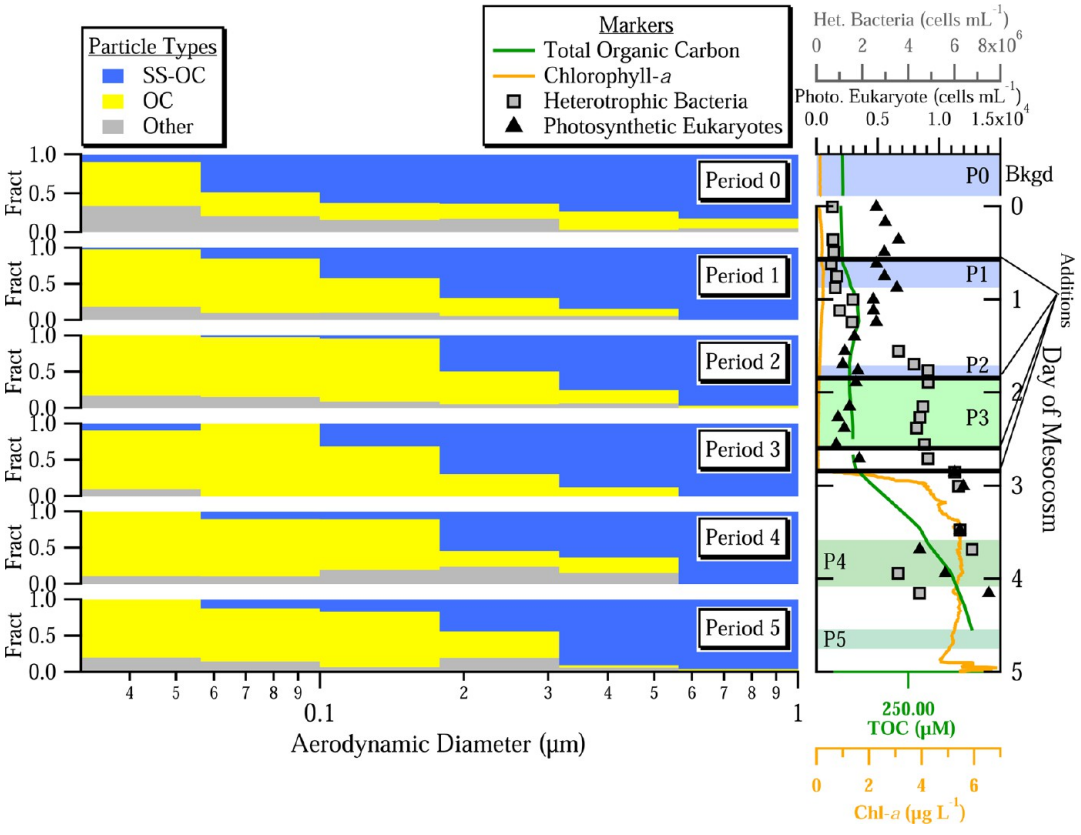

Figure 6. Size-resolved plots of the different particles present as a function of time during a mesocosm experiment. The time series on the right side shows additions of bacteria, phytoplankton, and oceanic growth media and the subsequent changes in different indicators of chemical complexity (heterotrophic bacteria, photosynthetic eukaryotes, TOC (total organic carbon), and Chl-*a* (Chlorophyll-*a*) as a function of time (increasing toward the bottom of the plot). The size-resolved compositional data on the left side of the figure correspond to several time periods labeled as Periods 0 through 5, which are also highlighted in blue or green behind the time series on the right-hand side.

dx.doi.org/10.1021/es400416g | Environ. Sci. Technol. 2013, 47, 5603−5612

of loss of a total chloride signal as observed here.[55] Thus, due to this lack of chloride and the different particle morphology, the particles labeled OC indicate a distinctly different particle type from SS-OC particles. The lack of chloride in OC particles is an interesting chemical observation. These data may suggest that carboxylic acid groups, a weak-acid moiety within the organic matter as shown by STXM, is reacting with chloride to yield gas-phase HCl via a mechanism for chloride displacement in salt particles recently proposed and observed by Laskin et al.[59] Whether or not this HCl elimination chemistry is occurring after aerosol production and collection, or another mechanism is operative leading to the lack of chloride in these particles, it is worthy of further investigation.

Although these studies strived to remove all other ambient particles, periods existed with increased concentrations up to 15% of particles sampled came from the ambient environment. This is due to ambient aerosol concentrations that were 2−3 orders of magnitude greater than SSA particle concentrations produced in these experiments.[28] By the end of the experiment, background levels represented less than 5% of the total particles. Two particle types observed in these experiments are thought to be due to background aerosol contamination, as discussed in Prather et al.[28] One type of contamination particle displays the characteristics of elemental carbon/soot, while another was identified as ammonium sulfate (AS) (shown as Particle 3 in Figure 4). Further information on these two particle types is given in the SI (Figures S3 and S4). The contamination types were easily identified because of the clean, controlled nature of the wave flume experimental apparatus, contrasting field measurements where determining oceanic versus anthropogenic origin is much more difficult.[60]

Size Resolved Chemical Composition as a Function of Increasing Seawater Complexity. As discussed above, different types of particles are observed across the broad size range from 30 nm to 10 μm. One important issue to address is how do these distinct particle populations vary as a function of size and seawater composition, particularly below 1 μm. A five day mesocosm experiment was conducted that began with natural seawater, followed by the addition of bacteria, phytoplankton, and growth media to increase seawater chemical complexity.[28] The increase in heterotrophic bacteria (HBact), photosynthetic eukaryotes (PEuk), total organic carbon (TOC), and chlorophyll-*a* (chl-*a*) are shown on the right-hand side of Figure 6, with time during the experiment increasing downward. These time series show the transition from natural seawater conditions to elevated TOC and chl-*a* concentrations, replicating conditions of a bloom, after the addition of bacteria, ZoBell growth media, and phytoplankton. Size resolved chemical composition data are shown in the left portion of Figure 6 starting with a background time period labeled Period 0 (top) and additional time periods later labeled Periods 1−5. Particles not in the SS-OC and OC classes, such as contamination particles, are grouped together in the "other" class. From 300 nm to 1 μm, the internally mixed SS-OC particle type represents greater than 80% of particles present under all conditions investigated. Conversely in the smallest size bin, 30−60 nm, OC particle types represent greater than 80% of particles during all conditions. It is important to note that in contrast to some previous studies,[24] NaCl-containing particles with an organic coating (SS-OC types) were observed at sizes below 200 nm (Figures 3 and 6). A major finding of these experiments is that the relative fraction of SS-OC decreases at smaller sizes (less than 200 nm) as bacterial and phytoplankton concentrations increased.

For larger particles, a key difference in SS-OC particles before and after the addition of bacteria and phytoplankton is the morphology of the NaCl core. Prior to the addition of bacteria and phytoplankton, NaCl shows a well-defined cubic crystal structure, whereas after addition of bacteria and phytoplankton the NaCl core becomes less cubic and more rounded. To quantify the particle morphology, the circularity, *C*, of each particle is defined in eqn. (2). Circularity distributions are shown in Figure 7a (before addition of bacteria and phytoplankton) and 7b (after addition of bacteria and phytoplankton) for particles across different size ranges. Above 1 μm prior to addition of bacteria and phytoplankton, the particles are more cubic with the maximum of the distribution, C_{max}, at 0.79, which shifts to a C_{max} of 0.84 below 1 μm. For reference, a circle has $C = 1$ and a square has $C = 0.79$. After addition of bacteria and phytoplankton, the particles become more spherical and the C_{max} is 0.91. Two factors explain the differences in these distributions. (1) The relative amount of organic matter in the SS-OC particles increases with decreasing size,[54] leading to less cubic particles before the addition of bacteria and phytoplankton below 1 μm. (2) After addition of bacteria and phytoplankton there is enough organic matter at all sizes to disrupt cubic crystal formation and the distribution does not shift as a function of size ($C_{max} = 0.93$). These data suggest that sodium chloride particles with minimal external species (OC, Mg, bound water, etc.) form the cubic crystals and that there is a critical amount of these other species that are needed to disrupt cubic crystallization.[59] The organic modification of the habit of crystallization of NaCl is a well-known process,[61] and has been

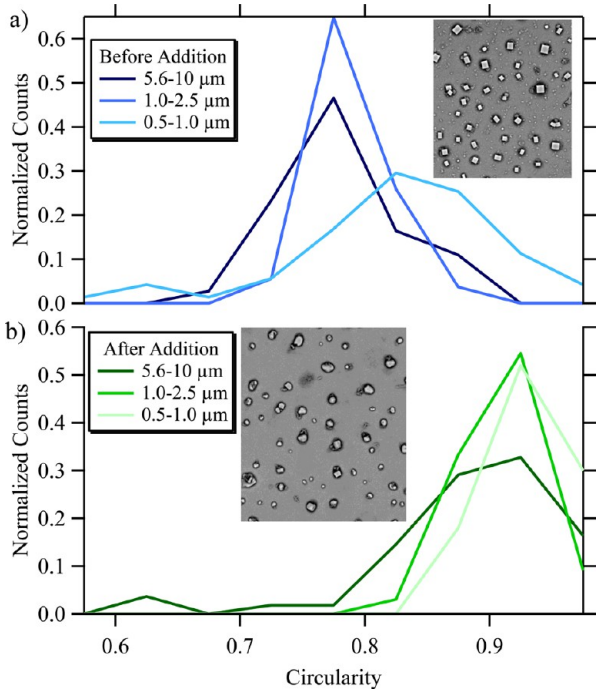

Figure 7. Circularity, *C*, as defined in the text, is shown for different size ranges (a) before and (b) after the addition of bacteria and phytoplankton. Images from before and after the additions are inset showing a change in the morphology of the NaCl away from a cubic structure. For reference, *C* is 1.0 for a sphere and 0.79 for a cube.

dx.doi.org/10.1021/es400416g | Environ. Sci. Technol. 2013, 47, 5603−5612

shown specifically for glycine and polysaccharides to lead to more rounded crystal structures, such as rhombic dodecahedron.[62,63] Finally, the broad width of the circularity distributions suggests that there is a diverse population of particles within SS-OC types that contain varying amounts of organic matter present across the sub- and supermicrometer size ranges.

■ ATMOSPHERIC IMPLICATIONS

The complexity of marine aerosols and their formation has challenged scientists since the middle of the last century.[64,65] By bringing the ocean to the laboratory, the CAICE intensive measurements described here were able to isolate nascent SSA particles, while systematically altering the seawater composition from which particles were formed. The measurements shown herein focus on identifying the different types of particles and variations in composition and structure within different subpopulations across a wide range of particle sizes from 30 nm to 10 μm using combined microscopy and spectroscopy probes. Within the two distinct types of aerosols observed in the submicrometer range (SS-OC and OC), there was a wide range of distinct morphologies, as well as relative amounts and distribution of species within individual particles. After the addition of bacteria, the fraction of the distinct OC subpopulation increased below 300 nm, while the relative contributions of SS-OC and OC were similar above 300 nm. However, within the SS-OC subpopulation above 500 nm, NaCl cores are more spherical in nature after addition of bacteria and phytoplankton, indicating an inhibition of cubic crystallization of the NaCl core by organic material, water, and hygroscopic salts such as $MgCl_2$. The results presented in this work demonstrate the variability of distinct particle types and heterogeneity within specific types as a function of size and seawater chemistry. The climate implications, such as changes in the cloud activation properties, due to these physicochemical changes are discussed in a separate publication.[47] These findings provide insight regarding ocean-atmosphere-climate linkages in marine environments that can be used to help improve the process of representing nascent sea spray aerosols in atmospheric chemistry and global climate modeling.

■ ASSOCIATED CONTENT

Supporting Information

Additional figures, table, and references not included in the text. This material is available free of charge via the Internet at http://pubs.acs.org.

■ AUTHOR INFORMATION

Corresponding Author

*E-mail: vicki-grassian@uiowa.edu (V.H.G.); kprather@ucsd.edu (K.A.P.).

Notes

The authors declare no competing financial interest.

■ ACKNOWLEDGMENTS

The authors wish to acknowledge all collaborators involved in the CAICE intensive measurement period. The staff of the SIO Hydraulics Laboratory is gratefully acknowledged for technical assistance during the campaign. The authors acknowledge the Central Microscopy Research Facility (CMRF) at the University of Iowa for assistance with microscopy measurements. This work was funded under the NSF Center for Chemical Innovation (CCI) grant CHE1038028. Any opinions, findings, and conclusions or recommendations expressed in this material are those of the authors and do not necessarily reflect the views of the National Science Foundation.

■ REFERENCES

(1) Andreae, M. O.; Rosenfeld, D. Aerosol−cloud−precipitation interactions. Part 1. The nature and sources of cloud-active aerosols. *Earth-Sci. Rev.* **2008**, *89* (1−2), 13−41.

(2) Forster, P.; Ramaswamy, V.; Artaxo, P.; Berntsen, T.; Betts, R.; Fahey, D. W.; Haywood, J.; Lean, J.; Lowe, D. C.; Myhre, G.; Nganga, J.; Prinn, R.; Raga, G.; Schulz, M.; Dorland, R. V. Changes in atmospheric constituents and in radiative forcing. In *Climate Change 2007: The Physical Science Basis. Contribution of Working Group I to the Fourth Assessment Report of the Intergovernmental Panel on Climate Change*; Cambridge University Press: New York, 2007.

(3) de Leeuw, G.; Andreas, E. L.; Anguelova, M. D.; Fairall, C. W.; Lewis, E. R.; O'Dowd, C.; Schulz, M.; Schwartz, S. E. Production flux of sea spray aerosol. *Rev. Geophys.* **2011**, *49*, RG000349.

(4) O'Dowd, C. D.; De Leeuw, G. Marine aerosol production: a review of the current knowledge. *Philos. Trans. R. Soc. London Ser. A-Math. Phys. Eng. Sci.* **2007**, *365* (1856), 1753−1774.

(5) Carslaw, K. S.; Boucher, O.; Spracklen, D. V.; Mann, G. W.; Rae, J. G. L.; Woodward, S.; Kulmala, M. A review of natural aerosol interactions and feedbacks within the Earth system. *Atmos. Chem. Phys.* **2010**, *10* (4), 1701−1737.

(6) Long, M. S.; Keene, W. C.; Kieber, D. J.; Erickson, D. J.; Maring, H. A sea-state based source function for size- and composition-resolved marine aerosol production. *Atmos. Chem. Phys.* **2011**, *11* (3), 1203−1216.

(7) Furutani, H.; Dall'osto, M.; Roberts, G. C.; Prather, K. A. Assessment of the relative importance of atmospheric aging on CCN activity derived from field observations. *Atmos. Environ.* **2008**, *42* (13), 3130−3142.

(8) Blanchard, D. C. Sea-to-air transport of surface active material. *Science* **1964**, *146* (364), 396−397.

(9) Facchini, M. C.; Rinaldi, M.; Decesari, S.; Carbone, C.; Finessi, E.; Mircea, M.; Fuzzi, S.; Ceburnis, D.; Flanagan, R.; Nilsson, E. D.; de Leeuw, G.; Martino, M.; Woeltjen, J.; O'Dowd, C. D. Primary submicron marine aerosol dominated by insoluble organic colloids and aggregates. *Geophys. Res. Lett.* **2008**, *35* (17), L034210.

(10) Cavalli, F.; Facchini, M. C.; Decesari, S.; Mircea, M.; Emblico, L.; Fuzzi, S.; Ceburnis, D.; Yoon, Y. J.; O'Dowd, C. D.; Putaud, J. P.; Dell'Acqua, A. Advances in characterization of size-resolved organic matter in marine aerosol over the North Atlantic. *J. Geophys. Res.-Atmos.* **2004**, *109* (D24), D005137.

(11) Ceburnis, D.; Garbaras, A.; Szidat, S.; Rinaldi, M.; Fahrni, S.; Perron, N.; Wacker, L.; Leinert, S.; Remeikis, V.; Facchini, M. C.; Prevot, A. S. H.; Jennings, S. G.; Ramonet, M.; O'Dowd, C. D. Quantification of the carbonaceous matter origin in submicron marine aerosol by ^{13}C and ^{14}C isotope analysis. *Atmos. Chem. Phys.* **2011**, *11* (16), 8593−8606.

(12) Keene, W. C.; Maring, H.; Maben, J. R.; Kieber, D. J.; Pszenny, A. A. P.; Dahl, E. E.; Izaguirre, M. A.; Davis, A. J.; Long, M. S.; Zhou, X.; Smoydzin, L.; Sander, R. Chemical and physical characteristics of nascent aerosols produced by bursting bubbles at a model air-sea interface. *J. Geophys. Res.-Atmos.* **2007**, *112* (D21), D008464.

(13) Wells, M. L.; Goldberg, E. D. Occurence of small colloids in sea-water. *Nature* **1991**, *353* (6342), 342−344.

(14) Hedges, J. I.; Eglinton, G.; Hatcher, P. G.; Kirchman, D. L.; Arnosti, C.; Derenne, S.; Evershed, R. P.; Kogel-Knabner, I.; de Leeuw, J. W.; Littke, R.; Michaelis, W.; Rullkotter, J. The molecularly-uncharacterized component of nonliving organic matter in natural environments. *Org. Geochem.* **2000**, *31* (10), 945−958.

(15) Kovac, N.; Bajt, O.; Faganeli, J.; Sket, B.; Orel, B. Study of macroaggregate composition using FT-IR and H-1-NMR spectroscopy. *Mar. Chem.* **2002**, *78* (4), 205−215.

(16) Kovac, N.; Faganeli, J.; Bajt, O.; Sket, B.; Orel, B.; Penna, N. Chemical composition of macroaggregates in the northern Adriatic sea. *Org. Geochem.* **2004**, *35* (10), 1095−1104.
(17) Chin, W. C.; Orellana, M. V.; Verdugo, P. Spontaneous assembly of marine dissolved organic matter into polymer gels. *Nature* **1998**, *391* (6667), 568−572.
(18) Verdugo, P. Marine Microgels. In *Annual Review of Marine Science, Vol 4*, Carlson, C. A.; Giovannoni, S. J., Eds.; **2012**; Vol. *4*, pp 375−400.
(19) Verdugo, P.; Alldredge, A. L.; Azam, F.; Kirchman, D. L.; Passow, U.; Santschi, P. H. The oceanic gel phase: A bridge in the DOM-POM continuum. *Mar. Chem.* **2004**, *92* (1−4), 67−85.
(20) Orellana, M. V.; Matrai, P. A.; Leck, C.; Rauschenberg, C. D.; Lee, A. M.; Coz, E. Marine microgels as a source of cloud condensation nuclei in the high Arctic. *Proc. Natl. Acad. Sci. U. S. A.* **2011**, *108* (33), 13612−13617.
(21) Vignati, E.; Facchini, M. C.; Rinaldi, M.; Scannell, C.; Ceburnis, D.; Sciare, J.; Kanakidou, M.; Myriokefalitakis, S.; Dentener, F.; O'Dowd, C. D. Global scale emission and distribution of sea-spray aerosol: Sea-salt and organic enrichment. *Atmos. Environ.* **2010**, *44* (5), 670−677.
(22) Rinaldi, M.; Decesari, S.; Finessi, E.; Carbone, C.; Mircea, M.; Fuzzi, S.; Ceburnis, D.; O'Dowd, C. D.; Facchini, M. C. Marine organic aerosol: Characterization by proton nuclear magnetic resonance spectroscopy (^{1}H NMR). *Geochim. Cosmochim. Acta* **2009**, *73* (13), A1102−A1102.
(23) McNeill, V. F.; Patterson, J.; Wolfe, G. M.; Thornton, J. A. The effect of varying levels of surfactant on the reactive uptake of N_2O_5 to aqueous aerosol. *Atmos. Chem. Phys.* **2006**, *6*, 1635−1644.
(24) Bigg, E. K.; Leck, C. The composition of fragments of bubbles bursting at the ocean surface. *J. Geophys. Res.-Atmos.* **2008**, *113* (D11), D009078.
(25) Quinn, P. K.; Bates, T. S. The case against climate regulation via oceanic phytoplankton sulphur emissions. *Nature* **2011**, *480* (7375), 51−56.
(26) Clarke, A. D.; Owens, S. R.; Zhou, J. C. An ultrafine sea-salt flux from breaking waves: Implications for cloud condensation nuclei in the remote marine atmosphere. *J. Geophys. Res.-Atmos.* **2006**, *111* (D6), D006565.
(27) Murphy, D. M.; Anderson, J. R.; Quinn, P. K.; McInnes, L. M.; Brechtel, F. J.; Kreidenweis, S. M.; Middlebrook, A. M.; Posfai, M.; Thomson, D. S.; Buseck, P. R. Influence of sea-salt on aerosol radiative properties in the Southern Ocean marine boundary layer. *Nature* **1998**, *392* (6671), 62−65.
(28) Prather, K. A.; Bertram, T. H.; Grassian, V. H.; Deane, G. B.; Stokes, M. D.; DeMott, P. J.; Aluwihare, L. I.; Palenik, B. P.; Azam, F.; Seinfeld, J. H.; Moffet, R. C.; Molina, M. J.; Cappa, C. D.; Geiger, F. M.; Roberts, G. C.; Russell, L. M.; Ault, A. P.; Baltrusaitis, J.; Collins, D. B.; Corrigan, C. E.; Cuadra-Rodriguez, L. A.; Ebben, C. J.; Forestieri, S. D.; Guasco, T. L.; Hersey, S. P.; Kim, M. J.; Lambert, W. F.; Modini, R. L.; Mui, W.; Pedler, B. E.; Ruppel, M. J.; Ryder, O. S.; Schoepp, N. G.; Sullivan, R. C.; Zhao, D. Bringing the ocean into the laboratory to probe the chemical complexity of sea spray aerosol. *Proc. Natl. Acad. Sci. U. S. A.* **2013**, *110* (19), 7550−7555.
(29) Gantt, B.; Meskhidze, N.; Facchini, M. C.; Rinaldi, M.; Ceburnis, D.; O'Dowd, C. D. Wind speed dependent size-resolved parameterization for the organic mass fraction of sea spray aerosol. *Atmos. Chem. Phys.* **2011**, *11* (16), 8777−8790.
(30) Decesari, S.; Finessi, E.; Rinaldi, M.; Paglione, M.; Fuzzi, S.; Stephanou, E. G.; Tziaras, T.; Spyros, A.; Ceburnis, D.; O'Dowd, C.; Dall'Osto, M.; Harrison, R. M.; Allan, J.; Coe, H.; Facchini, M. C. Primary and secondary marine organic aerosols over the North Atlantic Ocean during the MAP experiment. *J. Geophys. Res.-Atmos.* **2011**, *116*, D016204.
(31) Deane, G. B.; Stokes, M. D. Scale dependence of bubble creation mechanisms in breaking waves. *Nature* **2002**, *418* (6900), 839−844.
(32) Oppenheimer, C. H.; Zobell, C. E. The growth and viability of 63 species of marine bacteria as influenced by hydrostatic pressure. *J. Mar. Res.* **1952**, *11* (1), 10−18.
(33) Hansell, D. A.; Carlson, C. A.; Repeta, D. J.; Schlitzer, R. Dissolved organic matter in the ocean a controversy stimulates new insights. *Oceanography* **2009**, *22* (4), 202−211.
(34) Li, W. K. W. Annual average abundance of heterotrophic bacteria and *Synechococcus* in surface ocean waters. *Limnol. Oceanogr.* **1998**, *43* (7), 1746−1753.
(35) Boyce, D. G.; Lewis, M. R.; Worm, B. Global phytoplankton decline over the past century. *Nature* **2010**, *466* (7306), 591−596.
(36) Moffet, R. C.; Henn, T.; Laskin, A.; Gilles, M. K. Automated Chemical Analysis of Internally Mixed Aerosol Particles Using X-ray Spectromicroscopy at the Carbon K-Edge. *Anal. Chem.* **2010**, *82* (19), 7906−7914.
(37) Kilcoyne, A. L. D.; Tyliszczak, T.; Steele, W. F.; Fakra, S.; Hitchcock, P.; Franck, K.; Anderson, E.; Harteneck, B.; Rightor, E. G.; Mitchell, G. E.; Hitchcock, A. P.; Yang, L.; Warwick, T.; Ade, H. Interferometer-controlled scanning transmission X-ray microscopes at the Advanced Light Source. *J. Synchrotron Radiat.* **2003**, *10*, 125−136.
(38) Hinds, W. C. *Aerosol Technology: Properties, Behavior, And Measurements of Airborne Particles*; Wiley: New York, 1999.
(39) Ott, D. K.; Cyrs, W.; Peters, T. A. Passive measurement of coarse particulate matter, PM10−2.5. *J. Aerosol Sci.* **2008**, *39* (2), 156−167.
(40) Wagner, J.; Leith, D. Passive aerosol sampler. Part I: Principle of operation. *Aerosol Sci. Technol.* **2001**, *34* (2), 186−192.
(41) Kuwata, M.; Zorn, S. R.; Martin, S. T. Using elemental ratios to predict the density of organic material composed of carbon, hydrogen, and oxygen. *Environ. Sci. Technol.* **2012**, *46* (2), 787−794.
(42) Kuwata, M.; Kondo, Y. Measurements of particle masses of inorganic salt particles for calibration of cloud condensation nuclei counters. *Atmos. Chem. Phys.* **2009**, *9* (16), 5921−5932.
(43) Conny, J. M.; Norris, G. A. Scanning electron microanalysis and analytical challenges of mapping elements in urban atmospheric particles. *Environ. Sci. Technol.* **2011**, *45* (17), 7380−7386.
(44) Ault, A. P.; Peters, T. M.; Sawvel, E. J.; Casuccio, G. S.; Willis, R. D.; Norris, G. A.; Grassian, V. H. Single-particle SEM-EDX analysis of iron-containing coarse particulate matter in an urban environment: Sources and distribution of iron within Cleveland, Ohio. *Environ. Sci. Technol.* **2012**, *46* (8), 4331−4339.
(45) Liu, Y.; Yang, Z.; Desyaterik, Y.; Gassman, P. L.; Wang, H.; Laskin, A. Hygroscopic behavior of substrate-deposited particles studied by micro-FT-IR spectroscopy and complementary methods of particle analysis. *Anal. Chem.* **2008**, *80* (3), 633−642.
(46) Russell, L. M.; Hawkins, L. N.; Frossard, A. A.; Quinn, P. K.; Bates, T. S. Carbohydrate-like composition of submicron atmospheric particles and their production from ocean bubble bursting. *Proc. Natl. Acad. Sci. U. S. A.* **2010**, *107* (15), 6652−6657.
(47) Collins, D. B.; Ault, A. P.; Ruppel, M. J.; Cuadra-Rodriguez, L. A.; Guasco, T. L.; Corrigan, C. E.; Moffet, R. C.; Pedler, B.; Azam, F.; Aluwihare, L. I.; Bertram, T. H.; Roberts, G. C.; Grassian, V. H.; Prather, K. A. Chemical mixing state impacts the cloud activity of nascent sea spray aerosol. *J. Geophys. Res.-Atmos.* **2013**, submitted.
(48) Liu, Y.; Minofar, B.; Desyaterik, Y.; Dames, E.; Zhu, Z.; Cain, J. P.; Hopkins, R. J.; Gilles, M. K.; Wang, H.; Jungwirth, P.; Laskin, A. Internal structure, hygroscopic and reactive properties of mixed sodium methanesulfonate-sodium chloride particles. *Phys. Chem. Chem. Phys.* **2011**, *13* (25), 11846−11857.
(49) Tong, H. J.; Qian, Z. G.; Reid, J. P.; Zhang, Y. H. High temporal and spatial resolution measurements of the rapid efflorescence of sea salt droplets. *Acta Phys.-Chim. Sin.* **2011**, *27* (11), 2521−2527.
(50) Bertram, T. H.; Thornton, J. A. Toward a general parameterization of N_2O_5 reactivity on aqueous particles: The competing effects of particle liquid water, nitrate, and chloride. *Atmos. Chem. Phys.* **2009**, *9* (21), 8351−8363.
(51) Hawkins, L. N.; Russell, L. M. Polysaccharides, proteins, and phytoplankton fragments: four chemically distinct types of marine

primary organic aerosol classified by single particle spectromicroscopy. *Adv. Met.* **2010**, 612132.
(52) Hopkins, R. J.; Desyaterik, Y.; Tivanski, A. V.; Zaveri, R. A.; Berkowitz, C. M.; Tyliszczak, T.; Gilles, M. K.; Laskin, A. Chemical speciation of sulfur in marine cloud droplets and particles: Analysis of individual particles from the marine boundary layer over the California current. *J. Geophys. Res.-Atmos.* **2008**, *113* (D4), D008954.
(53) Chen, Y. Z.; Shah, N.; Huggins, F. E.; Huffman, G. P. Microanalysis of ambient particles from Lexington, KY, by electron microscopy. *Atmos. Environ.* **2006**, *40* (4), 651−663.
(54) Ault, A. P.; Zhao, D.; Ebben, C. J.; Tauber, M. J.; Geiger, F. M.; Prather, K. A.; Grassian, V. H. Raman microspectroscopy and vibrational sum frequency generation spectroscopy as probes of the bulk and surface compositions of size-resolved sea spray aerosol particles. *Phys. Chem. Chem. Phys.* **2013**, *15* (17), 6206−6214.
(55) Krueger, B. J.; Grassian, V. H.; Iedema, M. J.; Cowin, J. P.; Laskin, A. Probing heterogeneous chemistry of individual atmospheric particles using scanning electron microscopy and energy-dispersive X-ray analysis. *Anal. Chem.* **2003**, *75* (19), 5170−5179.
(56) Pilson, M. E. Q. *An Introduction to the Chemistry of the Sea*; Prentice Hall: New York, 1998.
(57) Li, J.; Anderson, J. R.; Buseck, P. R. TEM study of aerosol particles from clean and polluted marine boundary layers over the North Atlantic. *J. Geophys. Res.-Atmos.* **2003**, *108* (D6), D002106.
(58) Lide, D. R., Ed. *CRC Handbook of Chemistry and Physics*, 89th ed.; CRC Press/Taylor and Francis: Boca Raton, FL, 2009.
(59) Laskin, A.; Moffet, R. C.; Gilles, M. K.; Fast, J. D.; Zaveri, R. A.; Wang, B. B.; Nigge, P.; Shutthanandan, J. Tropospheric chemistry of internally mixed sea salt and organic particles: Surprising reactivity of NaCl with weak organic acids. *J. Geophys. Res.-Atmos.* **2012**, *117*, D017743.
(60) Bates, T. S.; Quinn, P. K.; Frossard, A. A.; Russell, L. M.; Hakala, J.; Petaja, T.; Kulmala, M.; Covert, D. S.; Cappa, C. D.; Li, S. M.; Hayden, K. L.; Nuaaman, I.; McLaren, R.; Massoli, P.; Canagaratna, M. R.; Onasch, T. B.; Sueper, D.; Worsnop, D. R.; Keene, W. C. Measurements of ocean derived aerosol off the coast of California. *J. Geophys. Res.-Atmos.* **2012**, *117*, D017588.
(61) de Rome de l'Isle, J. B. L. *Cristallographie*; Paris, 1783; p 379.
(62) Birchall, J. D.; Davey, R. J. The crystallization of sodium chloride from aqueous sollution in the presence of polysaccharides. *J. Cryst. Growth* **1981**, *54* (2), 323−329.
(63) Ballabh, A.; Trivedi, D. R.; Dastidar, P.; Ghosh, P. K.; Pramanik, A.; Kumar, V. G. A practical approach to produce near-spherical common salt crystals with better flow characteristics. *Cryst. Growth Des.* **2006**, *6* (7), 1591−1594.
(64) Blanchard, D. C.; Woodcock, A. H. Bubble formation and modification in the sea and its meteorological signficance. *Tellus* **1957**, *9* (2), 145−158.
(65) Woodcock, A. H.; Gifford, M. M. Sampling atmospheric sea-salt nuclei over the ocean. *J. Mar. Res.* **1949**, *8* (2), 177−197.